Journal of Engineering Mathematics **41:** 203–219, 2001.

Numerical simulation of sedimentation in the presence of 2D compressible convection and reconstruction of the particle-radius distribution function

K. V. PARCHEVSKY
Crimean Astrophysical Observatory, p/o Nauchny, Crimea 98409, Ukraine
(e-mail: kparchevsky@solar.stanford.edu)

Received 26 June 2000; accepted in revised form 21 June 2001

Abstract. Numerical simulation of the sedimentation of a polydisperse suspension in a convectively unstable medium is presented. For the simulation of 2D compressible convection, the full system of hydrodynamic equations is solved by the explicit MacCormack scheme. Velocities and positions of suspension particles are calculated simultaneously with the solution of the equations. Initially, the particles are randomly distributed in the computational region. The total weight of sedimented matter is recorded during the numerical experiment. The results are compared with the sedimentation of the same suspension without convection. To reconstruct the particle-radius distribution function from the sedimentation curve, a new method is used. This method is based on the solution of the sedimentation integral equation by the Tikhonov regularization method and was recently developed by the author. To illustrate this technique, sedimentation of cement powder in air is simulated. The suspension contains 50 000 particles. The particle radii are assumed to be log-normally distributed. Heat-driven convection is completely determined by the top and bottom boundary temperatures of the computational region and lateral boundary conditions. It is shown that convective motions of a medium with sedimented particles lead to the following effect: the fine disperse fraction of the suspension remains suspended much longer than without convection. Some particles will not sediment at all. The maximum radius of the particles of this fraction depends on the convection parameters (*e.g.* on convection cell size and convection velocities). These parameters, in their turn, depend only on the temperature difference of the top and bottom boundaries. The results of these calculations can be applied in geology and meteorology for studying dust sedimentation in air as well as in technology. Heat-driven convection can be used for separation of suspensions with the cut-off particle radius depending on temperature difference only.

Key words: convection, ill-posed problem, polydisperse suspension, sedimentation, Tikhonov regularization.

1. Introduction

Sedimentation processes play an important role in a wide variety of fields in applied physics as well as in technology for separation and purification. Many technological processes use sedimentation for the size separation of the particles of a suspension. The study of the settling behavior of polydisperse suspensions is a matter of great importance. The size spectrum of particles is an important attribute of polydisperse suspensions. The sedimentation curve (the weight of settled particles versus time) is widely used for the reconstruction of the particle-radius distribution function. The usual technique of obtaining the particle-radius distribution function is based on the construction of tangent lines to the sedimentation curve and measuring the tangent line intercepts (see below). This graphic method gives only a rough histogram and cannot be used for reconstructing small-scale details of the radius distribution function. For example, it cannot resolve close peaks of the radius distribution function for a mixture

of suspensions. The low accuracy of this method can be explained as follows. When we construct the tangent lines, we use information about the sedimentation curve in the vicinity of the tangency points only, ignoring other points of the curve. Experimental errors are always present in the observed data. These errors lead to the great uncertainty in the slope angle of the tangent line if we use only local information. The other common methods one way or the other also lead to unstable solutions. The problem of reconstruction of the particle-radius distribution function from the sedimentation curve represents a clear example of so-called *ill-posed inverse problems*. Special regularizing procedures were developed to solve such problems. Each regularizing procedure essentially uses additional *a priori* information about the solution. This information is not contained in the experimental data and must be imposed by the researcher. Different methods of regularization require for their implementation different amounts of additional information. Algorithms which require minimum additional information are preferable. Hence, we need a new method for the reconstruction of the particle-radius distribution function which meets to the following requirements: (1) the method must yield a continuous smooth solution (instead of a rough histogram); (2) the method must be global and should use all information contained in the sedimentation curve; (3) the method must use a regularizing algorithm to stabilize the solution. Such a new method based on the solution of an integral equation is proposed in this paper. The Tikhonov regularization algorithm is used to stabilize the solution. This method requires minimum *a priori* information: (1) smoothness of the solution; (2) values of the experimental errors.

Very often particles settle in a non-static medium. Sometimes medium motions have a preferred direction such as in pipe flow, in some cases they do not, for instance in the case of heat convection. In technology unwelcome medium motions can be reduced, but in many cases motions are significant and have to be taken into account. Convection flows are driven by temperature gradients. If we do not make special efforts to stabilize the temperature, convection arises almost everywhere. In this case, a knowledge of convection influences on the sedimentation process would be extremely welcome.

How does convection distort the result of the reconstruction of the particle-radius distribution function? During sedimentation all particles are separated into two fractions: settled and suspended. What is the shape of the size spectrum of suspension particles in these fractions? To answer these questions, direct numerical simulations of the settling of polydisperse suspensions are done in this paper.

2. The reconstruction of the particle-radius distribution function

Let us consider the sedimentation of a polydisperse suspension. Assume, that the suspension particles have the same density and do not interact each other. We introduce the radius distribution function of particles $q(r)$ in such a way that $q(r)\,\mathrm{d}r$ represents the mass fraction of particles with radii in a range from r to $r + \mathrm{d}r$. By definition the function $q(r)$ is normalized as follows:

$$\int_0^\infty q(r)\,\mathrm{d}r = 1\,. \tag{1}$$

We assume that the particles of the suspension settle at a constant velocity

$$u = \frac{2}{9}\frac{\Delta\rho}{\eta} g r^2\,, \tag{2}$$

where $\Delta\rho$ is the difference between the density of the particles and the liquid, g is the gravitational acceleration, and η is the viscosity of the liquid. We do not take into account a hindered settling discussed, for example, in [1]. It means, that results of the particle-radius reconstruction can be directly applied to the dilute suspensions.

Assume that we measure the weight of particles settled on the solid surface at a depth H. All particles with a settling velocity

$$u \geq \frac{H}{t}$$

(or, equivalently, with radii $r \geq r^*$), will settle at the moment of time t. The radius r^* is given by the formula

$$r^* = \sqrt{\frac{9\eta H}{2\Delta\rho g t}} \,. \tag{3}$$

Then we introduce the mass fraction of totally settled particles Q as

$$Q = \int_{r^*}^{\infty} q(r)\,\mathrm{d}r = 1 - \int_0^{r^*} q(r)\,\mathrm{d}r \,. \tag{4}$$

Particles with radii $r < r^*$ will settle partially. Let us consider the suspension fraction with particle radii in the range from r to $r + \mathrm{d}r$. The mass fraction of these particles is equal to $q(r)\,\mathrm{d}r$ and their settling velocity is given by Equation (2). Only particles which are initially near the bottom in the column of liquid $h = ut$ in height will settle at time t. Hence, the mass fraction of the partially settled particles with radii between r and $r + \mathrm{d}r$ equals

$$\mathrm{d}S = \frac{h}{H} q(r)\,\mathrm{d}r = \frac{2}{9}\frac{\Delta\rho}{\eta}\frac{g}{H} t q(r) r^2\,\mathrm{d}r \,.$$

The mass fraction of the partially settled particles with radii $0 < r < r^*$ is given by the finite integral

$$S = \frac{2}{9}\frac{\Delta\rho}{\eta}\frac{g}{H} t \int_0^{r^*} q(r) r^2\,\mathrm{d}r \,. \tag{5}$$

The total mass fraction of the settled particles is equal to

$$P = Q + S = 1 - \int_0^{r^*} q(r)\,\mathrm{d}r + \frac{2}{9}\frac{g\Delta\rho}{\eta H} t \int_0^{r^*} q(r) r^2\,\mathrm{d}r \,. \tag{6}$$

One can rewrite Equation (6) in the following form

$$\int_0^{r^*(t)} q(r) \left[1 - \left(\frac{r}{r^*(t)}\right)^2\right] \mathrm{d}r = 1 - P(t) \,. \tag{7}$$

The value $P(t)$ in the right-hand side of Equation (7) is known from the experiment (with some error). Hence, we can consider Equation (7) as an integral equation for the radius distribution function $q(r)$. Taking the second time derivative from both sides of Equation (7), one can obtain a formal solution of the integral equation

$$q(r^*) = -2\frac{t^2}{r^*}\frac{\mathrm{d}^2}{\mathrm{d}t^2} P(t) \,. \tag{8}$$

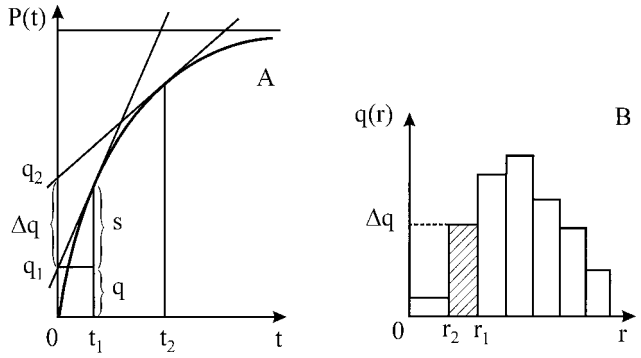

Figure 1. Graphic method for the reconstruction of the particle-radius distribution from the sedimentation curve. Tangent line intercepts q_i represent the mass fractions of totally settled particles at the corresponding moments of time. The interval $|q_2 - q_1|$ represents the mass fraction of suspended particles with the radii in the range between r_1 and r_2.

The common method of reconstructing the particle-size distribution function from the sedimentation curve is the following. One can draw tangent lines to the sedimentation curve $P(t)$ (see Figure 1a). The tangent line intercept q represents the mass fraction of totally settled particles at the corresponding moment of time t. Hence, the interval $|q_2 - q_1|$ represents the mass fraction of suspended particles with the radii in the range between r_1 and r_2. The particle equivalent radius is given by Equation (3), where t must be taken equal to the abscissa of the tangency point. This procedure is no more than an application of Equation (8) with the graphical method of calculation of the second derivative. Nothing but a rough histogram (see Figure 1b) can be obtained by this method. We need a method which will give a possibility of reconstructing a *smooth* size-distribution function, using a sedimentation curve that will be free from the inaccuracies of the graphical method. There are two approaches to the solution of this problem: a) to solve directly the integral Equation (7) with respect to $q(r)$; b) to calculate numerically the derivative of the second order from the sedimentation curve and to substitute it in Equation (8).

When we use the second approach, it is implied that we know how to calculate correctly the second derivative from the noisy experimental data correctly. Calculation of the derivative from an experimental function $f(x)$ obtained with errors represents a complicated mathematical problem. The main difficulty is the following. During the experiment we can measure only a function $f(x) + \varepsilon$, where ε is a noise. The second term does not have a derivative in the classical meaning. If we make an attempt to calculate the derivative by the usual methods, we shall obtain an alternating-sign saw-tooth function of high amplitude and the real derivative $f'(x)$ will 'sink' in the noise generated by the second term. The problem of derivative reconstruction from experimental data is discussed in detail in [2, 3]. It is shown that special regularization algorithms must be used for obtaining a smooth derivative. The appropriate method is the following. One can write an integral equation for the second derivative as

$$\int_a^x (x - \xi) f''(\xi)\, \mathrm{d}\xi = f(x) - f(a) - f'(x)|_{x=a}(x - a)\,. \tag{9}$$

So, we can see that both approaches to the reconstruction of the particle-radius distribution are reduced to the solution of the following Volterra integral equation of the first kind:

$$Ay \equiv \int_a^x K(x,\xi)y(\xi)\,\mathrm{d}\xi = f(x)\ . \tag{10}$$

The first equality sign in Equation (10) can be considered as the definition of the integral operator A. If we use the first approach (a) and solve the integral equation (7), the kernel $K(x,\xi)$ and the right-hand side $f(x)$ in Equation (10) must be chosen as follows:

$$K(t,r) = 1 - \left(\frac{r}{r^*(t)}\right)^2\ , \quad f(t) = 1 - P(t)\ . \tag{11}$$

In the second approach (b), using the formal solution (8), we must calculate the second derivative first. To obtain the derivative, we have to solve Equation (10) with the following kernel and the right-hand side

$$K(t,\xi) = t - \xi, \quad f(t) = P(t) - P(0) - P'(t)|_{t=0}t\ . \tag{12}$$

It is shown [4] that the first approach is more preferable because it gives a more stable solution.

3. Tikhonov regularization

The concept of ill- (or well-) posed problems goes back to the work of J. Hadamard [5, 6]. A problem is called well-posed if (1) a solution of the problem exists, (2) the solution is unique, (3) the solution is stable (this means that small variations of the initial data give rise to small variations of the solution). If any one of these conditions is violated, the problem is called ill-posed.

The Volterra equation of the first kind has (in some sense) an intermediate position between the Volterra equation of the second kind and the Fredholm equation of the first kind. The Volterra equation of the second kind is well-posed and can be solved by classical methods. The Fredholm equation of the first kind is ill-posed in any 'reasonable' functional spaces and must be solved by special regularizing algorithms. The Volterra equation of the first kind can be either ill- or well-posed, depending on the function spaces where we seek a solution. However, even in the case when the problem is well-posed, some methods of solution can lead to instability. It can be shown [7, 8, pp. 110–114] that the quadrature methods based on Simpson, Newton–Cotes and other formulas of high order generate divergent algorithms, even for the well-posed problems. Rectangle or trapezoid formulas are stable only if we choose the step of integration in a particular way, depending on errors in the right-hand side and the kernel. In this case, the quadrature method can be treated as a regularizing algorithm where the step of integration plays a role of the regularizing parameter. This fact imposes a strict limitation on the use of this method because usually the right-hand side of the integral equation (10) is known from the experiment in the form of a table with an irregular step. So, to obtain values of the right-hand side in the nodes of the regular grid with optimal step, we have to solve a nontrivial (in a general case) problem of interpolation or approximation (for example by splines) of the experimental data.

The Volterra integral equation of the first kind can be treated as a special case of the Fredholm integral equation of the first kind, which is ill-posed. Special regularizing algorithms have been developed for the solution of such equations. These algorithms can be directly applied to the solution of a Volterra integral equation of the first kind as well. We used the Tikhonov regularization method [9, pp. 128–158] to solve the integral equation (10). There

is an English translation of this book [10]. This method is more powerful and flexible than 'regularized' quadrature formulas and does not require choosing a special step of integration.

Initially, this method was developed for the solution of Fredholm integral equations of the first kind

$$\begin{aligned} &\int_a^b K(x,\xi)y(\xi)\,\mathrm{d}\xi = f(x), \quad c \le x \le d\ , \\ &f(x) \in L_2[c,d], \quad K(x,\xi) \in L_2[a,b]\times[c,d], \quad y(\xi) \in D \subseteq W_2^1[a,b]\ . \end{aligned} \tag{13}$$

Here D is the closed convex set of *a priori* limitations of the problem, such that $0 \in D$. Assume, that instead of the exact kernel $K(x,\xi)$ and the right-hand side $f(x)$ we know their approximate values $K_h(x,\xi)$ and $f_\delta(x)$ so that

$$\left\| f_\delta - f \right\|_{L_2} \le \delta, \quad \left\| K_h - K \right\|_{L_2} \le h\ ,$$

i.e. actually we solve the following equation

$$\int_a^b K_h(x,\xi)y(\xi)\,\mathrm{d}\xi = f_\delta(x), \quad c \le x \le d\ . \tag{14}$$

Assume that the exact solution $y(x)$ is continuous and has a quadratically integrable derivative on $[a,b]$. Hence, A_h operates from $W_2^1[a,b]$ to $L_2[c,d]$. In the Tikhonov regularization method a solution $y(x)$ of Equation (14) is sought as a function which minimizes the following functional:

$$M^\alpha[y] = \left\| A_h y - f_\delta \right\|_{L_2}^2 + \alpha \left\| y \right\|_{W_2^1}^2\ . \tag{15}$$

The optimal value of the regularizing parameter α^* can be found as a solution of the nonlinear algebraic equation [11, pp. 55–59]

$$\rho(\alpha^*) \equiv \left\| A_h y^\alpha - f_\delta \right\|^2 - (\delta + h\left\| y^\alpha \right\| + \mu)^2 = 0\ , \tag{16}$$

where $\rho(\alpha)$ is the so-called *generalized residual*, and μ is the measure of incompatibility of the initial integral equation (14). It is defined as follows:

$$\mu = \inf_{y\in D}(\delta + h\left\| y \right\| + \left\| A_h y - f_\delta \right\|)\ . \tag{17}$$

For details of the numerical realization of this algorithm for the reconstruction of the particle-size distribution function see [4]. This technique is universal and can be applied to the solution of any Fredholm integral equation of the first kind. On the one hand, universality permits us to use the same procedure in both approaches (a) and (b) of the reconstruction of the particle-radius distribution function; on the other hand, it does not take into account some *a priori* information about the reconstructed distribution. For example, this technique does not preserve the positivity of the distribution. A modification of the mathematical procedure of the reconstruction to preserve the positivity of the solution, simultaneously with taking into account a hindered settling in Equation (7), will be done in future work.

4. Governing hydrodynamic equations

The technique of reconstructing the particle-radius distribution function based on the solution of an ill-posed inverse problem of sedimentation described above assumes that the medium is

static. Convection (if present) distorts the reconstruction result. Since there is no adequate analytical description of convection, it cannot be taken into account directly in Equation (7). So we are forced to simulate this process numerically. Let us consider the following model. The suspension particles settle in a viscous compressible medium. The particles do not interact. The particle velocity

$$\mathbf{v}_{\text{particle}} = \mathbf{v}_{\text{settle}} + \mathbf{v}_{\text{medium}}$$

has two components: a constant settling rate $\mathbf{v}_{\text{settle}}$, given by Equation (2), and the hydrodynamic velocity of medium motion $\mathbf{v}_{\text{medium}} = (u, v)$. The evolution of a viscous compressible medium is described by the full system of hydrodynamic equations

$$\begin{cases} \dfrac{\partial \rho}{\partial t} + \dfrac{\partial}{\partial x}(\rho u) + \dfrac{\partial}{\partial y}(\rho v) = 0 \,, \\ \dfrac{\partial}{\partial t}(\rho u) + \dfrac{\partial}{\partial x}(\rho u^2 + \dfrac{p}{\gamma} - \tau_{xx}) + \dfrac{\partial}{\partial y}(\rho u v - \tau_{xy} = 0) \,, \\ \dfrac{\partial}{\partial t}(\rho v) + \dfrac{\partial}{\partial x}(\rho u v - \tau_{xy}) + \dfrac{\partial}{\partial y}(\rho v^2 + \dfrac{p}{\gamma} - \tau_{yy}) + \dfrac{\rho}{\mathrm{Fr}^2} = 0 \,, \\ \dfrac{\partial \mathrm{E}}{\partial t} + \dfrac{\partial}{\partial x}\left[u(E + \dfrac{p}{\gamma} - \tau_{xx}) - v\tau_{xy} + \dot{Q}_x\right] + \\ \qquad \dfrac{\partial}{\partial y}\left[v(E + \dfrac{p}{\gamma} - \tau_{yy}) - u\tau_{xy} + \dot{Q}_y\right] + \dfrac{\rho v}{\mathrm{Fr}^2} = 0 \,, \end{cases} \tag{18}$$

where τ_{ij} is the viscous stress tensor given by

$$\tau_{xx} = \frac{2}{3}\frac{1}{\mathrm{Re}}\left(2\frac{\partial u}{\partial x} - \frac{\partial v}{\partial y}\right), \quad \tau_{yy} = \frac{2}{3}\frac{1}{\mathrm{Re}}\left(2\frac{\partial v}{\partial y} - \frac{\partial u}{\partial x}\right), \quad \tau_{xy} = \tau_{yx} = \frac{1}{\mathrm{Re}}\left(\frac{\partial u}{\partial y} + \frac{\partial v}{\partial x}\right) .$$

Heat-transfer rates can be written in accordance with the Fourier law

$$\dot{Q}_x = -\frac{1}{\mathrm{Re}\ \mathrm{Pr}(\gamma - 1)}\frac{\partial T}{\partial x}, \quad \dot{Q}_y = \frac{1}{\mathrm{Re}\ \mathrm{Pr}(\gamma - 1)}\frac{\partial T}{\partial y} .$$

Using the equation of state for an ideal gas, $p = \rho T$, we can express the pressure p in terms of the total energy per unit volume, E, as follows:

$$p = \gamma(\gamma - 1)\left(E - \frac{(\rho u)^2 + (\rho v)^2}{2\rho}\right) ,$$

where $\gamma = \mathrm{c_p}/\mathrm{c_v}$ is the adiabatic exponent, ρ is the density, u and v are the x and y velocity components of the medium. The dimensionless parameters Re, Pr and Fr, given by the following expressions

$$\mathrm{Re} = \frac{\rho_0 a_0 L}{\eta}, \quad \mathrm{Pr} = \frac{\eta c_p}{k}, \quad \mathrm{Fr}^2 = \frac{a_0^2}{gL} ,$$

represent the Reynolds, Prandtl and Froude numbers, respectively, where η is the viscosity, k is the thermal conductivity, g is the gravitational acceleration, a is the sound velocity, and L is the characteristic size of the computational region. The subscript 0 shows that the values are related to some reference state. The state of matter at the top end of the computational domain is chosen as a reference state. All equations are written in terms of dimensionless variables:

$$x \to \frac{x}{L}, \quad t \to \frac{a_0}{L}t, \quad \rho \to \frac{\rho}{\rho_0}, \quad p \to \frac{p}{p_0},$$

$$u \to \frac{u}{a_0}, \quad T \to \frac{T}{T_0}, \quad T_0 \to \frac{p_0}{\rho_0 R}, \quad a_0^2 = \frac{\gamma p_0}{\rho_0},$$

where R is the gas constant.

Flows described by the full viscous system of hydrodynamic equations are mostly turbulent. The turbulent viscosity η_{T} and the turbulent thermal conductivity k_{T} were introduced to take into account the effects of turbulence

$$\eta_{\mathrm{T}} = \rho\Delta^2\sqrt{\left(\frac{\partial u}{\partial y}\right)^2 + \left(\frac{\partial v}{\partial x}\right)^2}, \quad k_{\mathrm{T}} = \frac{c_p\eta_{\mathrm{T}}}{\mathrm{Pr}_{\mathrm{T}}},$$

where Δ is the mixing length, Pr_{T} is the turbulent Prandtl number ($\mathrm{Pr}_{\mathrm{T}} = 0{\cdot}9$ for air). Since we want to simulate subgrid turbulence, Δ represents a characteristic grid-cell size and $\Delta^2 = \Delta x\Delta y$. To add a turbulence to the dimensionless equations (18), the following changes are necessary:

$$\frac{1}{\mathrm{Re}} \to \frac{1}{\mathrm{Re}} + \frac{1}{\mathrm{Re}_{\mathrm{T}}}, \frac{1}{\mathrm{Re\,Pr}} \to \frac{1}{\mathrm{Re\,Pr}} + \frac{1}{\mathrm{Re}_{\mathrm{T}}\mathrm{Pr}_{\mathrm{T}}},$$

$$\frac{1}{\mathrm{Re}_{\mathrm{T}}} = \frac{\eta_{\mathrm{T}}}{\rho_0 a_0 L} = C\rho\Delta^2\sqrt{\left(\frac{\partial u}{\partial y}\right)^2 + \left(\frac{\partial v}{\partial x}\right)^2},$$

where $C = 0{\cdot}2$ is an empirical dimensionless constant.

5. The MacCormack numerical scheme

The governing equations are written in divergence form and can be rewritten as a single vector equation as

$$\frac{\partial \mathbf{q}}{\partial t} + \frac{\partial \mathbf{F}}{\partial x} + \frac{\partial \mathbf{G}}{\partial y} + \mathbf{S} = 0. \tag{19}$$

The vector $\mathbf{q} = (\rho, \rho\mathrm{u}, \rho\mathrm{v}, E)^{\mathrm{T}}$ contains the independent variables. An explicit MacCormack scheme [12, pp. 479–483] can be directly applied to Equation (19) as follows:

Predictor step :

$$\mathbf{q}^*_{j,k} = \mathbf{q}^n_{j,k} - \frac{\Delta t}{\Delta x}(\mathbf{F}^n_{j+1,k} - \mathbf{F}^n_{j,k}) - \frac{\Delta t}{\Delta y}(\mathbf{G}^n_{j,k+1} - \mathbf{G}^n_{j,k}) - \Delta t\mathbf{S}^n_{j,k}, \tag{20}$$

$$\mathbf{F}^n_{j,k}: \begin{matrix} 0 \le j \le N_x + 1 \\ 0 \le k \le N_y \end{matrix} \quad \mathbf{G}^n_{j,k}: \begin{matrix} 0 \le j \le N_x \\ 0 \le k \le N_y + 1 \end{matrix} \quad \begin{matrix} 0 \le j \le N_x \\ 0 \le k \le N_y \end{matrix},$$

Corrector step :

$$\mathbf{q}^{n+1}_{j,k} = \frac{1}{2}\left[\mathbf{q}^n_{j,k} + \mathbf{q}^*_{j,k} - \frac{\Delta t}{\Delta x}(\mathbf{F}^*_{j,k} - \mathbf{F}^*_{j-1,k}) - \frac{\Delta t}{\Delta y}(\mathbf{G}^*_{j,k} - \mathbf{G}^*_{j,k-1}) - \Delta t\mathbf{S}^*_{j,k}\right], \tag{21}$$

$$\mathbf{F}^*_{j,k}: \begin{matrix} 0 \le j \le N_x - 1 \\ 1 \le k \le N_y - 1 \end{matrix} \quad \mathbf{G}^*_{j,k}: \begin{matrix} 1 \le j \le N_x - 1 \\ 0 \le k \le N_y - 1 \end{matrix} \quad \begin{matrix} 1 \le j \le N_x - 1 \\ 1 \le k \le N_y - 1 \end{matrix}.$$

The derivatives $\partial\mathbf{F}/\partial x$ and $\partial\mathbf{G}/\partial y$ in Equation (19) in the predictor step are approximated by the forward one-sided finite-difference operators. Quantities $\mathbf{F}$ and $\mathbf{G}$ in their turn also contain space derivatives $\partial/\partial x$ and $\partial/\partial y$. In general, the numerical scheme has accuracy of the second-order accuracy in both space and time if the following conditions are satisfied. For the approximation of $\partial/\partial x$ in $\mathbf{F}(\partial/\partial y$ in $\mathbf{G})$ in the predictor step the backward one-sided finite-difference operator is used. The derivative $\partial/\partial y$ in $\mathbf{F}(\partial/\partial x$ in $\mathbf{G})$ must be approximated by the central finite-difference operator. In the corrector step the finite-difference operators which approximate the derivatives $\partial/\partial x$ and $\partial/\partial y$ in $\mathbf{F}^*$ and $\mathbf{G}^*$ must be opposite to those used for the approximation of $\partial\mathbf{F}^*/\partial x$ and $\partial\mathbf{G}^*/\partial y$. The remaining derivatives must be approximated by the central differences. Explicit formulae for the approximation of $\mathbf{F}$ and $\mathbf{F}^*$ are the following:

$$\mathbf{F}^n_{jk} = \begin{pmatrix} (\rho u)^n_{jk} \\ (\rho u^2)^n_{jk} + \dfrac{p^n_{jk}}{\gamma} - \dfrac{2}{3}\dfrac{1}{\mathrm{Re}}\left(2\dfrac{u^n_{jk}-u^n_{j-1,k}}{\Delta x} - \dfrac{\nu^n_{j,k+1}-\nu^n_{j,k-1}}{2\Delta x}\right) \\ (\rho u\nu)^n_{jk} - \dfrac{1}{\mathrm{Re}}\left(\dfrac{u^n_{j,k+1}-u^n_{j,k-1}}{2\Delta y} + \dfrac{\nu^n_{jk}-\nu^n_{j-1,k}}{\Delta x}\right) \\ u^n_{jk}\left[E^n_{jk} + \dfrac{p^n_{jk}}{\gamma} - \dfrac{2}{3}\dfrac{1}{\mathrm{Re}}\left(2\dfrac{u^n_{jk}-u^n_{j-1,k}}{\Delta x} - \dfrac{\nu^n_{j,k+1}-\nu^n_{j,k-1}}{2\Delta y}\right)\right] - \\ \qquad \dfrac{\nu^n_{jk}}{\mathrm{Re}}\left(\dfrac{u^n_{j,k+1}-u^n_{j,k-1}}{2\Delta y} + \dfrac{\nu^n_{jk}-\nu^n_{j-1,k}}{\Delta x}\right) - \dfrac{1}{\mathrm{Re}\,\mathrm{Pr}(\gamma-1)}\dfrac{T^n_{jk}-T^n_{j-1,k}}{\Delta x} \end{pmatrix}, \tag{22}$$

$$\mathbf{F}^*_{jk} = \begin{pmatrix} (\rho u)^*_{jk} \\ (\rho u^2)^*_{jk} + \dfrac{p^*_{jk}}{\gamma} - \dfrac{2}{3}\dfrac{1}{\mathrm{Re}}\left(2\dfrac{u^*_{j+1,k}-u^*_{jk}}{\Delta x} - \dfrac{\nu^*_{j,k+1}-\nu^*_{j,k-1}}{2\Delta y}\right) \\ (\rho u\nu)^*_{jk} - \dfrac{1}{\mathrm{Re}}\left(\dfrac{u^*_{j,k+1}-u^n_{j,k-1}}{2\Delta y} + \dfrac{\nu^*_{j+1,k}-\nu^*_{jk}}{\Delta x}\right) \\ u^*_{jk}\left[E^*_{jk} + \dfrac{p^*_{jk}}{\gamma} - \dfrac{2}{3}\dfrac{1}{\mathrm{Re}}\left(2\dfrac{u^*_{j+1,k}-u^*_{jk}}{\Delta x} - \dfrac{\nu^*_{j,k+1}-\nu^*_{j,k-1}}{2\Delta y}\right)\right] - \\ \qquad \dfrac{\nu^*_{jk}}{\mathrm{Re}}\left(\dfrac{u^*_{j,k+1}-u^*_{j,k-1}}{2\Delta y} + \dfrac{\nu^*_{j+1,k}-\nu^*_{jk}}{\Delta x}\right) - \dfrac{1}{\mathrm{Re}\,\mathrm{Pr}(\gamma-1)}\dfrac{T^*_{j+1,k}-T^*_{jk}}{\Delta x} \end{pmatrix}. \tag{23}$$

Similar formulae can be written down for the finite-difference approximation of $\mathbf{G}$ and $\mathbf{G}^*$. As for any explicit scheme, numerical stability of the MacCormack scheme imposes a limitation on the choice of the time step. For the compressible Navier-Stokes equations, when $\Delta x = \Delta y$, it is recommended [12, p. 482] to use the following estimate of the time step:

$$\Delta t \le \Delta x^2 \left[\frac{2\eta}{\mathrm{Re}\rho}\left(\frac{2\gamma}{\mathrm{Pr}} + \sqrt{\frac{2}{3}}\right) + \Delta x\left(|u| + |\nu| + a\sqrt{2}\right)\right]^{-1}, \tag{24}$$

where a is the sound velocity.

6. Initial and boundary conditions

Assume, that the medium is enclosed in a rectangular box with the solid top and bottom walls. The box is heated from below bottom. Convection is driven by a temperature gradient between top and bottom boundaries where the following Dirichlet boundary conditions are imposed:

$$\begin{aligned}&\text{top boundary}: \quad T_{j,Ny}=1, \qquad u_{j,Ny}=0, \;\; \nu_{j,Ny}=0,\\ &\text{bottom boundary}: \; T_{j,0}=1+\Delta T, \qquad u_{j,0}=0, \quad \nu_{j,0}=0.\end{aligned}$$

Let us define how to calculate the velocity gradients at the top and bottom boundaries. For the approximation of $\partial/\partial y$ by a central finite-difference operator we must to extend the computational region, introducing non-physical nodes $(j,-1)$ and $(j,Ny+1)$ for $j=0,1,\ldots,N_x$. Using the interpolation one can find the velocities in the non-physical nodes as follows:

$$\begin{aligned}&\tfrac{1}{2}(u_{j,1}+u_{j,-1})=u_{j,0}\equiv 0, \qquad \tfrac{1}{2}(u_{j,Ny-1}+u_{j,Ny+1})=u_{j,Ny}\equiv 0,\\ &u_{j,-1}=-u_{j,1}, \qquad u_{j,Ny+1}=-u_{j,Ny-1}.\end{aligned}$$

Similar formulae can be written for the y-component. Now it is easy to write the central finite-difference approximation for the derivatives as

$$\left.\frac{\partial u}{\partial y}\right|_{j,0}=\frac{u_{j,1}-u_{j,-1}}{2\Delta y}=\frac{u_{j,1}}{\Delta y}, \quad \left.\frac{\partial u}{\partial y}\right|_{j,Ny}=\frac{u_{j,Ny-1}-u_{j,Ny+1}}{2\Delta y}=\frac{u_{j,Ny-1}}{\Delta y},$$

$$\left.\frac{\partial v}{\partial y}\right|_{j,0}=\frac{v_{j,1}-v_{j,-1}}{2\Delta y}=\frac{v_{j,1}}{\Delta y}, \quad \left.\frac{\partial v}{\partial y}\right|_{j,Ny}=\frac{v_{j,Ny-1}-v_{j,Ny+1}}{2\Delta y}=\frac{v_{j,Ny-1}}{\Delta y}.$$

Boundary conditions for the pressure and density must be consistent with the hydrodynamic equations in the interior points of the computational grid. The boundary-layer equations give us $\partial p/\partial y=0$. Taking into account that the temperature is constant at the top and bottom boundaries, we can write the following expressions for the physical quantities in the non-physical nodes of the computational grid:

bottom boundary	top boundary
$p_{j,-1}=p_{j,0}=p_{j,1}$,	$p_{j,Ny+1}=p_{j,Ny}=p_{j,Ny-1}$,
$T_{j,-1}=2T_{j,0}-T_{j,1}$, $T_{j,1}=\dfrac{p_{j,1}}{\rho_{j,1}}$,	$T_{j,Ny+1}=2T_{j,Ny}-T_{j,Ny-1}$, $T_{j,Ny-1}=\dfrac{p_{j,Ny-1}}{\rho_{j,Ny-1}}$,
$\rho_{j,-1}=\dfrac{p_{j,-1}}{T_{j,-1}}=\dfrac{p_{j,1}}{2T_{j,0}-T_{j,1}}$,	$\rho_{j,Ny+1}=\dfrac{p_{j,Ny+1}}{T_{j,Ny+1}}=\dfrac{p_{j,Ny-1}}{2T_{j,Ny}-T_{j,Ny-1}}$,
$E_{j,-1}=E_{j,0}+\dfrac{1}{2}\rho_{j,-1}(u_{j,1}^2+v_{j,1}^2)$,	$E_{j,Ny+1}=E_{j,Ny}+\dfrac{1}{2}\rho_{j,Ny+1}(u_{j,Ny-1}^2+v_{j,Ny-1}^2)$.

The lateral boundary conditions are assumed to be symmetrical as follows:

$$v_{\text{left}}=v_{\text{right}}, \quad u_{\text{left}}=-u_{\text{right}}.$$

Pressure, density, and temperature must be continuous on the lateral boundaries.

The initial conditions can be obtained as a solution of Equation (18) under the assumption that $u = v = 0$ everywhere in the computational domain. Under this assumption Equations (18) are reduced to the following system:

$$\frac{1}{\gamma}\frac{\partial p}{\partial y} + \frac{\rho}{\mathrm{Fr}^2} = 0, \qquad \frac{\partial^2 T}{\partial x^2} + \frac{\partial^2 T}{\partial y^2} = 0.$$

The initial state is static and does not depend on x. As follows from the temperature equation, the temperature T is a linear function of the depth y

$$T(t) = 1 + \Delta T(1 - y)\ . \tag{25}$$

Taking into account the equation of state, we can easily solve the pressure equation as

$$\begin{aligned} \rho(y) &= \left[1 + \Delta T(1 - y)\right]^{\frac{\gamma/\mathrm{Fr}^2 - \Delta T}{\Delta T}}, \\ p(y) &= \rho(y)T(y) = \left[1 + \Delta T(1 - y)\right]^{\frac{\gamma}{\Delta T\ \mathrm{Fr}^2}}. \end{aligned} \tag{26}$$

It should be noted that we use a system of units such that $T_{\mathrm{top}} = p_{\mathrm{top}} = \rho_{\mathrm{top}} = 1$.

To provide a 'soft' start of the convection without shock waves, we introduce an initial velocity field (div$\mathbf{v} = 0$) of a small amplitude A

$$u(x, y) = A \sin(2\pi x) \cos(\pi y),$$
$$v(x, y) = -A \cos(2\pi x) \sin(\pi y).$$

The velocity amplitude A is 10^5 times smaller than the final hydrodynamic velocities of the medium.

7. Results and discussion

We have simulated the sedimentation of cement polydisperse powder ($\rho_{\mathrm{particles}} = 2200$ kg/m^3) in air under the normal conditions. The square computational region with a side length of $L = 10$ m consists of 50×50 nodes of a uniform computational grid. The state of the medium at the top boundary (the reference state, denoted by subscript 0) is chosen as follows:

$T_0 = 273{\cdot}15$ K, $\quad \eta = 1{\cdot}98 \times 10^{-5}$ kg/m s,
$\rho_0 = 1{\cdot}333$ kg/m^3, $\quad \mathrm{Re} = 2{\cdot}2 \times 10^8$,
$p_0 = 101{\cdot}2$ kPa, $\quad \mathrm{Pr} = 0{\cdot}708$,
$a_0 = 326$ m/s, $\quad \mathrm{Fr} = 32{\cdot}931$.

It must be emphasized that this value of Re does not reflect a real condition of hydrodynamic similarity; it is just a coefficient in the hydrodynamic equations (18), based on the sound speed instead of the characteristic velocity. Accordingly, the medium velocities are measured in units of the sound speed. One can say in advance that the characteristic convective velocity under such conditions must be much smaller than the sound speed. The fact is that we do not know the characteristic velocity *before* calculation when we introduce the dimensionless parameters. The parameter Re which reflects a condition of hydrodynamic similarity can be

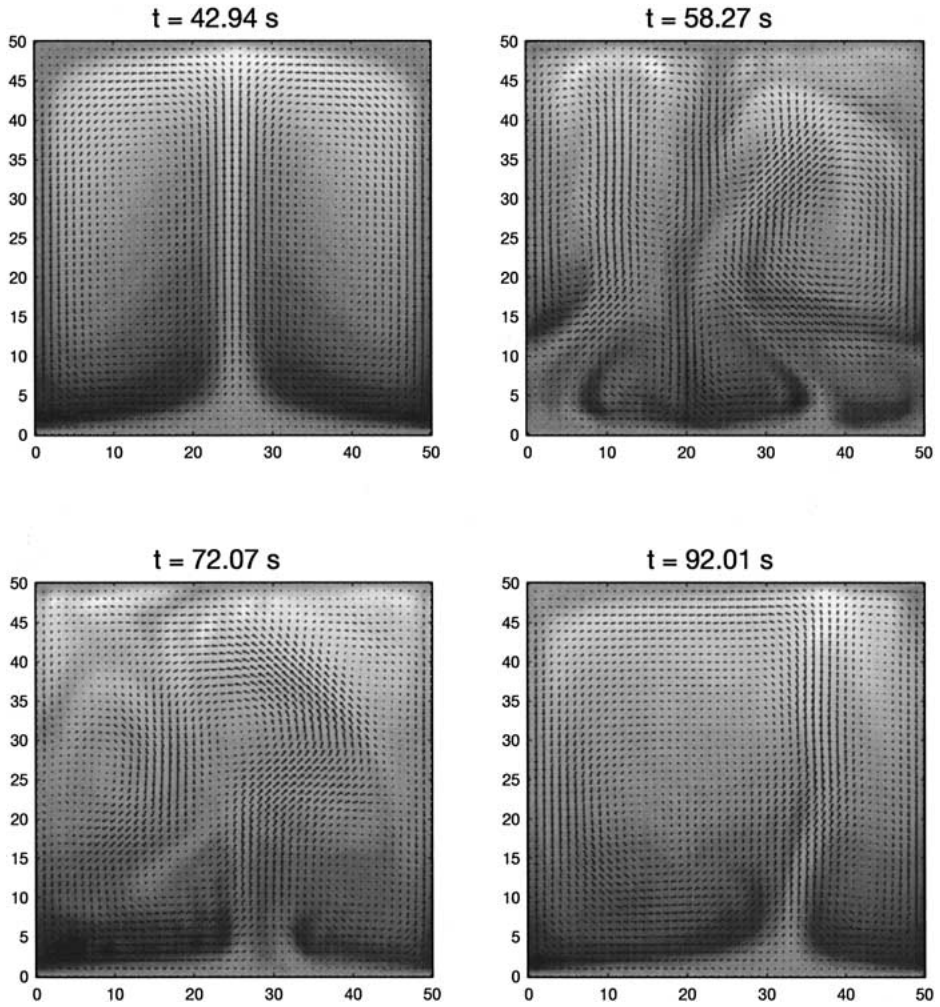

Figure 2. Snapshots of the computational region at different moments of simulation time during the transient process. Brightness denotes the difference between the temperature of the medium and the linear temperature distribution. Arrows show the amplitude and the direction of the medium velocities.

recalculated later when the maximum medium velocity will be known. The convection is driven by the temperature gradient between the top and bottom boundaries. The computational region is heated from the bottom. Calculations were carried out for two cases: $\Delta T = 20$ K and $\Delta T = 50$ K. The time step was chosen as $\Delta t = 1{\cdot}53 \times 10^{-4}$ s in accordance with Equation (24).

When a transient is completedfinished (after approximately 1·5 min. of simulation time), the hydrodynamic system reaches a quasi-steady state. This process for $\Delta T = 50$ K is illustrated by Figure 2. It consists of snapshots of the computational region at the different moments of simulation time. Each snapshot is a gray-scale map which shows the difference between the temperature of the medium and the initial temperature distribution given by Equation (25). Negative values (dark) denote that the temperature of the medium at this point is smaller than the initial temperature. Positive values (bright) indicate that the temperature is higher than in the case when there is no convection ($u = v = 0$). Arrows show the amplitude

and the direction of the medium velocities. The maximum medium velocity amplitude and the velocity components of the quasi-steady state are the following: $|\mathbf{V}_{\max}| = 1{\cdot}7$ m/s for $\Delta T = 50$ K and $|\mathbf{V}_{\max}| = 1{\cdot}1$ m/s for $\Delta T = 20$ K. Now we can recalculate the Reynolds number as $\mathrm{Re} = \rho_0 V_{\max} L/\eta = 1{\cdot}1 \times 10^6$.

When the quasi-steady state is reached, 50000 particles of the suspension are randomly distributed in the computational region. Usually, the suspension of small particles is made by breaking. It can be shown [13] that particles of such a suspension have a log-normal distribution of the radii. The particle radii of our suspension are assumed to be log-normally distributed:

$$q(r) = \frac{1}{r\sigma\sqrt{2\pi}} \exp\left[-\frac{1}{2}\left(\frac{\log r - \langle r\rangle}{\sigma}\right)^2\right] \tag{27}$$

with the following parameters $\langle r\rangle = 0, \sigma = 1/2$. The radii of the particles have been chosen in such a way that the settling time of a particle with the most probable radius from a height $L = 10$ m in a static medium is equal to 1 minute. For numerical simulation of the artificial sample of lognormally distributed particle radii, we start from a random value y that is uniformly distributed on the interval $0 \le y < 1$. This is a very important step. Most compilers contain built-in random-value generators. They are almost always *linear congruential generators* and they do not satisfy all requirements for random-number generators. They must never be used! We used the procedure ran1( ) from [14]. It uses a combination of three random generators with additional shuffle which breaks up serial correlations. To obtain a random value x with a predefined normalized density distribution function $q(x)$ from a uniformly distributed random number y, the following nonlinear equation must be solved with respect to x

$$\int_0^x q(\xi)\,\mathrm{d}\xi = y\ .$$

Positions of suspension particles are calculated by use of a simple Euler scheme simultaneously with the solution of the hydrodynamic equations (18). The total weight $P(t)$ of settled matter is recorded during the numerical experiment. Settled particles are excluded from the further calculations. All particles of the suspension are separated into two fractions: settled and suspended particles. On the one hand, the numerical simulation of the sedimentation in the convection medium gives us a sedimentation curve $P(t)$ (the weight of settled matter versus time); on the other hand, it gives us information about the radii of settled and suspended particles. If we want to study particle sizes of these two fractions, we have to know how to calculate the particle-radius distribution function when we have a sample of suspension particles.

The particle radius distribution function can be reconstructed directly from the sample of finite size in the following way. The proposed approach is based on the calculation of the first derivative from the empirical cumulative distribution function $F_e(x)$. The probability density distribution and cumulative distribution are related by the formula

$$\int_0^x q(\xi)\,\mathrm{d}\xi = F(x)\ . \tag{28}$$

To obtain $q(x)$ we have to substitute an empirical normalized cumulative distribution function

$$F_e(x) = \begin{cases} 0, & x < x_1, \\ \dfrac{i}{N}, & x_i \le x < x_{i+1}, \\ 1, & x \ge x_N \end{cases}$$

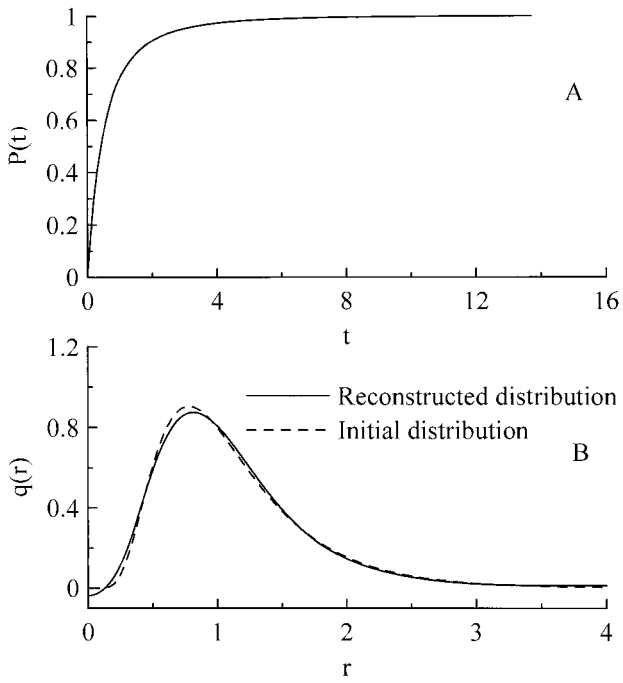

Figure 3. Application of the Tikhonov regularization procedure to the reconstruction of the particle-radius distribution from the sedimentation curve in the case of a static medium. Time and radius are given in normalized units.

calculated from the experimental sample $(x_1, x_2, \ldots, x_N)$, in the right-hand side of Equation (28) and to solve the integral equation. The Tikhonov regularization algorithm was used to solve this Volterra integral equation of the first kind.

Hence, the whole computational procedure consists of three steps: (1) numerical simulation of the convection until the system will reach a quasi-steady state; (2) numerical simulation of the sedimentation of a polydisperse suspension in the convectively unstable medium; (3) reconstruction of the particle-radius distribution from the sedimentation curve and from the samples of particle radii of both settled and suspended fractions.

For comparison, we simulated a sedimentation of the *same suspension* with the *same initial distribution* of particles in a static medium as well. Results of this simulation are shown in Figure 3. Figure 3a represents the simulated sedimentation curve. The dashed line in Figure 3b represents the initial particle-radius distribution (27). The solid line represents the particle-radius distribution reconstructed from the simulated sedimentation curve by solution of Equation (7). One can see a good agreement of the initial and reconstructed distributions.

The results of the numerical simulation of sedimentation in the presence of compressible convection are shown in Figure 4. For comparison, we present the result of sedimentation in a static medium in the same figure. The curves were simulated for two temperature differences of the top and bottom boundaries: $\Delta T = 20$ K and $\Delta T = 50$ K. The curves represent a mass fraction of settled matter versus time (time is given in normalized units). Asymptotes are calculated as follows. The curve $P(1/t)$ is extrapolated until it intercepts the OY axis. The ordinate of the intersection point gives us the desired value. The convective motion of the medium leads to the following effect. The fine dispersed fraction of the suspension remains suspended much longer than without convection. Some particles with sufficiently small radii

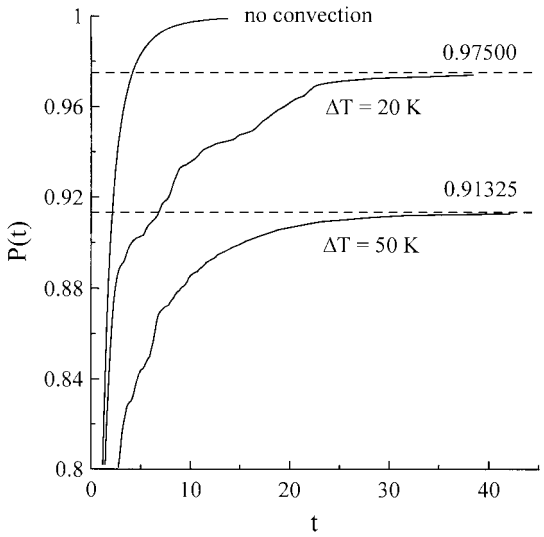

Figure 4. Sedimentation curves represent a mass fraction of settled matter versus time in the presence of 2D compressible heat-driven convection. Asymptotes show the mass fraction of the suspended particles whichthat will not settle. For comparison, a sedimentation curve of the same suspension in a static medium is added to the figure.

will not settle at all. The mass of the suspended fraction depends on the average convection velocities of the medium. Velocities in their turn depend only on the temperature difference of the top and bottom boundaries. The greater the temperature difference (and convection velocities), the greater the total mass of the suspended fraction.

The distribution of particle radii in settled and suspended fractions is a matter of great interest. During numerical simulation, the radii of settled particles are registered as well. So we have samples of radii of settled and airborne particles for every moment of time. The problem of the reconstruction of the particle-radius distribution is reduced to the problem of reconstructing the probability density distribution function from a sample of finite size and we can use the approach discussed above. Results of reconstructing the particle-radius distribution functions from the samples are shown in Figure 5. Dashed lines represent the particle-radius distribution in suspended and settled fractions. A solid line represents the initial particle-radius distribution.

Usually, the real experiment gives us only a sedimentation curve $P(t)$ and, perhaps, the sample of particles from the settled fraction, but not the sample of suspended particles. The procedure of reconstructing the particle-radius distribution function from the sedimentation curve described above assumes that the medium is static. Convective motions of the medium distort the result of reconstruction. If we apply this technique directly to the sedimentation curves in Figure 4, we do not obtain a real particle-radius distribution function, but such calculations could be helpful. The result of reconstructing the particle-radius distribution function from the sedimentation curves obtained in the presence of convection is presented in Figure 6. The dashed lines in Figure 6 represent particle-radius distributions obtained by solution of the integral equation (7). One can see a gap in the range of small radii, because these particles remain suspended and do not settle. It indicates a lack of particles with small radii. Convection acts as a size filter which separates particles on the basis of their radii. The average (and the most probable) particle radius of suspended and settled fractions depends on the parameters

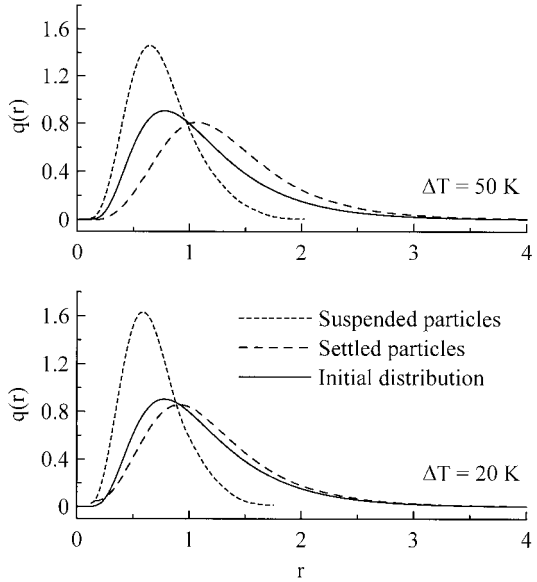

Figure 5. Numerical results of the reconstruction of the particle-radius distribution function from samples of suspension particles. The solid line represents the initial distribution. The dashed lines with the short and long dashes represent the particle-radius distribution in suspended and settled fractions, respectively.

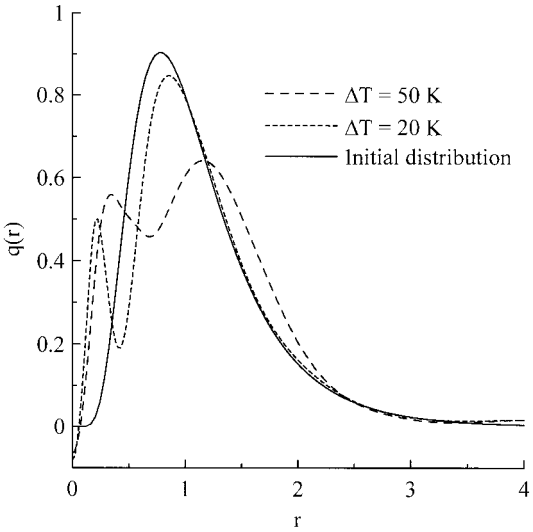

Figure 6. Numerical results of the reconstruction of the particle-radius distribution function from the sedimentation curve by the Tikhonov regularization method. The solid line represents the initial distribution. The dashed lines with the short and long dashes represent the particle-radius distribution reconstructed from the sedimentation curves in the presence of convection for the following temperature difference of the top and bottom boundaries, respectively: $\Delta T = 20$ K, $\Delta T = 50$ K.

of convection. These parameters, in their turn, depend *only* on the temperature difference of the top and bottom boundaries. It gives a possibility to develop a separation technology which is based on the simultaneous separation action of the sedimentation and convection. In such a method the cut-off particle radius will be controlled by choosing the appropriate temperature difference between the top and bottom boundaries.

8. Conclusions

In this paper we have proposed a new method for the reconstruction of the particle-radius function from the sedimentation curve. It was shown, that this problem is a special case of an ill-posed inverse problem. The new method is based on the solution of the integral equation of sedimentation by the Tikhonov regularization method. This approach gives a continuous smooth distribution function. The new method is flexible and very sensitive. It can be used for the reconstruction of the fine structure of the particle-radius distribution function. The main input parameter of this method is the error δ of the experimental data (error of the right-hand side of Equation (7)). Choosing the different values of this parameter we can control the degree of smoothness of the solution.

Convection distorts the results of the reconstruction of the particle-radius distribution function. In this case we are forced to use direct numerical simulation of the sedimentation process. Convection acts as a size filter and separates particles into settled and suspended fractions. The fine disperse fraction of the suspension remains suspended much longer, than without convection. Some particles with sufficiently small radii will not sediment at all. The maximal radius of particles of this fraction depends on parameters of the convection parameters (*e.g.*, on convection cell size and convection velocities). These parameters, in their turn, depend only on the temperature difference of the top and bottom boundaries. The results of this calculations can be applied in geology and meteorology for studying dust sedimentation in air as well as in the technology for separation of powders separation. Heat-driven convection can be used for the separation of a suspension with cut-off particle radius being dependent on temperature difference only.

Acknowledgements

The author acknowledges Prof. Dr.-Ing. W.L. Wendland and Dr. R. Bürger for a fruitful discussion on the reconstruction of the particle-radius distribution function from the sedimentation curve in a workshop on 'Mathematical Problems in Suspension Flows' in the framework of the Applied Mathematics for Industrial Flow AMIF Program of the European Science Foundation ESF.

References

1. V. Ramakrishna and S.R. Rao, Particle size determination and hindered settling. *J. Appl. Chem.* 15 (1965) 473–479.
2. K.V. Parchevsky, Using regularizing algorithms for the reconstruction of growth rate from the experimental data. *Ecol. Model.* 133 (2000) 107–115.
3. K.V. Parchevsky and V.P. Parchevsky, Determination of instantaneous growth rates using a cubic spline approximation. *Thermochim. Acta* 309 (1998) 181–192.
4. K.V. Parchevsky, A new method for the reconstruction of the particle radius distribution function from the sedimentation curve. *Chem. Eng. J.* 80 (2000) 73–79.
5. J. Hadamard, Sur les problèmes aux derivees partielles et leur signification physique. *Bull. Univ. Princeton,* 13 (1902) 49–52.
6. J. Hadamard, Le problème de Caucy et les équations aux derivees partielles linéaires huperboliques. Paris: Hermann, Paris, (1932) 352 pp.
7. A.S. Apartsin, About application of different quadrature formulas for numerical solution of Volterra integral equations of the first kind by quadrature sum method. *Differents. i Integr. Uravnenija* 2 (1973) 107–116 (in Russian).
8. A.F. Verlan and V.S. Sizikov, *Integral Equations: Methods, Algorythms, Programs*. Kiev: Naukova Dumka (1986) 544 pp. (in Russian).
9. A.N. Tikhonov and V.J. Arsenin, *Methods of Solution of Ill-posed Problems*. Moscow: Nauka (1979) 286 pp. (in Russian).
10. Tikhonov and V.J. Arsenin, *Solutions of iIll-Posed Problems*. Washington: Winston and Sons (1977) 258 pp.
11. A.N. Tikhonov, A.V. Goncharsky, V.V. Stepanov and A.G. Jagola, *Numerical Methods of Solution of Ill-posed Problems*. Moscow: Nauka (1990) 332 pp. (in Russian).
12. C.A.J. Fletcher, *Computational Techniques for Fluid Dynamics. Specific Techniques for Different Flow Categories*. Vol. 2. Berlin: Springer-Verlag (1988) 552 pp.
13. A.N. Kolmogorov, About logarithmically normal particle size distribution law at breaking. *Dokl. Akad. Nauk SSSR* 31 (1941) 99–101 (in Russian).
14. W.H. Press, S.A. Teukolsky, W.T. Vetterling, B.P. Flannery. *Numerical Recipes in C*. Cambridge: Cambridge University Press (1992) 998 pp.